https://ntrs.nasa.gov/search.jsp?R=19930087765 2020-06-17T12:01:20+00:00Z

N67 62201
335

CONFIDENTIAL

Copy
RM L53G22a

NACA RM L53G22a

NACA

CASE FILE
COPY

RESEARCH MEMORANDUM

LONGITUDINAL STABILITY CHARACTERISTICS AT TRANSONIC SPEEDS OF A ROCKET-PROPELLED MODEL OF AN AIRPLANE CONFIGURATION HAVING A 45° SWEPT WING OF ASPECT RATIO 6.0

By John C. McFall, Jr.

Langley Aeronautical Laboratory
Langley Field, Va.

CLASSIFICATION CHANGED TO UNCLASSIFIED
AUTHORITY: NACA RESEARCH ABSTRACT NO. 129
EFFECTIVE DATE: JULY 17, 1958
WHL

CLASSIFIED DOCUMENT

This material contains information affecting the National Defense of the United States within the meaning of the espionage laws, Title 18, U.S.C., Secs. 793 and 794, the transmission or revelation of which in any manner to an unauthorized person is prohibited by law.

NATIONAL ADVISORY COMMITTEE FOR AERONAUTICS

WASHINGTON

January 4, 1954

CONFIDENTIAL

NATIONAL ADVISORY COMMITTEE FOR AERONAUTICS

RESEARCH MEMORANDUM

LONGITUDINAL STABILITY CHARACTERISTICS AT TRANSONIC SPEEDS OF A ROCKET-PROPELLED MODEL OF AN AIRPLANE CONFIGURATION HAVING A 45° SWEPT WING OF ASPECT RATIO 6.0

By John C. McFall, Jr.

SUMMARY

A flight investigation has been conducted to determine the longitudinal characteristics of an airplane configuration having a 45° swept wing of aspect ratio 6.0, taper ratio of 0.6, and NACA 65A009 airfoil section. The variation of lift, drag, and pitch damping was closely similar to data from other sources investigating a swept, high-aspect-ratio, thick wing. No pitch-up was experienced by the low tail configuration of the present investigation.

INTRODUCTION

A rocket-propelled model of an airplane configuration having a 45° swept wing of aspect ratio 6.0 has been flown as a part of a general research program investigating longitudinal stability of an aircraft configuration having various wing plan forms and thicknesses. (See refs. 1 to 8.) The wing flown in this investigation had a taper ratio of 0.6 and an NACA 65A009 airfoil section. The configuration of the present model differed from previous models in this program by having a swept empennage with a low tail position for the longitudinal control surfaces. The model was flown at the Langley Pilotless Aircraft Research Station at Wallops Island, Va.

SYMBOLS

C_{N_A} model normal-force coefficient, $\frac{a_n}{g}\frac{W/S}{q}$

C_{N_W} exposed wing normal-force coefficient, $\frac{\text{Wing normal force}}{qS}$

C_C	chord-force coefficient, $-\frac{a_l}{g}\frac{W/S}{q}$
C_L	lift coefficient, $C_N \cos \alpha - C_C \sin \alpha$
C_{L_α}	lift-curve slope, per deg
C_D	drag coefficient, $C_C \cos \alpha + C_N \sin \alpha$
C_m	pitching-moment coefficient
C_{m_α}	slope of pitching-moment curve, per deg
C_{L_W}	exposed wing lift coefficient
a_n	normal acceleration as obtained from accelerometer, ft/sec^2
a_l	longitudinal acceleration as obtained from accelerometer, ft/sec^2
g	acceleration of gravity, ft/sec^2
$\bar{c}$	mean aerodynamic chord, ft
b	wing span, ft
$b_e/2$	exposed wing semispan, ft
p	free-stream static pressure, lb/sq ft
p_o	standard sea-level static pressure (2,116 lb/sq ft)
L	load applied, lb
K	factor for converting elastic wing lift data to rigid values
θ	local streamwise wing twist angle produced by L, radians; or model angle of pitch, deg
M	Mach number
S	wing area (including area enclosed within fuselage), sq ft

W	weight, lb
q	free-stream dynamic pressure, lb/sq ft
α	angle of attack, deg
δ	control-surface deflection; measured parallel to model center line with respect to chord plane of wing, deg
P	period of oscillation, sec
R	Reynolds number, based on wing mean aerodynamic chord
$T_{1/2}$	time to damp to one-half amplitude, sec
$C_{m_q} + C_{m_{\dot{\alpha}}}$	pitch damping coefficient, per radian

Subscripts:

t	trim
W	wing
A	complete model

$$q = \frac{d\theta}{dt}\frac{\bar{c}}{2V}$$

$$\dot{\alpha} = \frac{d\alpha}{dt}\frac{c}{2V}\frac{1}{57.3}$$

MODEL AND APPARATUS

Model

General dimensions of the model in the present investigation are presented in figure 1 by a drawing and in figure 2 by photographs.

The empennage section of the general configuration has been changed from that shown in reference 1 to that of the present investigation. The empennage of the present configuration has a vertical fin of wood and aluminum with the quarter-chord line swept 60° and NACA 65A003

airfoil section; and longitudinal control surfaces of Duralumin with 20° anhedral, 45° quarter-chord line sweep, and NACA 65A006 airfoil section.

The control surfaces were rotated about their 42-percent-chord lines in an approximate square-wave program by separate servos fed by the same pressure system and regulated by an electric-motor-driven selector valve. For the present investigation the control positions were at 0.1° and -3.5° measured parallel to the model center line.

The Duralumin wing in this investigation had an aspect ratio of 6.0, taper ratio of 0.6, quarter-chord sweep of 45°, and NACA 65A009 airfoil section. The fuselage ordinates of the present configuration are the same as those of reference 8.

The model weighed 148.3 pounds with a moment of inertia in pitch of 8.62 slug-feet^2 and had its center of gravity located at 0.25 of the wing mean aerodynamic chord.

Instrumentation

A 10-channel NACA telemeter was used to transmit continuous data from the model to the ground receiving station which recorded the information as light traces on photographic paper. A section of this telemeter record is shown in figure 3 with the traces of the measured quantities labeled. A description of the wing normal-force instrumentation (an inductance gage) may be found in reference 3. The quantity labeled "normal accelerometer (nose)" was intended for use in obtaining values of total pitching moment as in reference 8. The two-accelerometer method for obtaining total pitching moment was not used in the present investigation since the nose normal accelerometer trace was imposed on both by nose-shaking and wing-bending frequencies. The quantity labeled "downwash pressure" was experimental instrumentation and is not reported in the present investigation.

Radar units were used to obtain flight-path and velocity information. Atmospheric conditions at the time of the flight were determined using a radiosonde. Motion-picture cameras were used to photograph the launching and first portion of the flight.

Preflight Measurements

Twist in the free-stream direction per unit load applied at various loading stations along the 25- and 50-percent-chord lines of the wing is shown in figures 4(a) and 4(b), respectively. A photograph of the test equipment used may be found in reference 3. The factors obtained

through the use of this twist information (refs. 8 and 9) are presented in figure 5 for use in converting elastic wing lift-curve slope to rigid values, and for aerodynamic-center shift caused by the inboard movement of the aerodynamic load due to flexibility. These factors were not applied to the basic data.

The vibrational characteristics of the model were determined by recording the response of the model to vibrations of known frequency and to vibrations from striking the major components of the model such as nose, wing, vertical fin, and longitudinal control surfaces.

The measured vibrational characteristics of the model components were as follows:

Wing:

First bending, cps	28.5
Second bending, cps	135.0
Torsion, cps	310.0

Vertical fin:

First bending, cps	52.0

Control surface:

First bending, cps	92.0

Measurements of the weight of the moving parts of the wing and beam-type balance in which the wing was mounted (ref. 3) were made to be used in applying a correction for inertia effects on the wing normal-force data by the method of reference 3.

TESTS AND ANALYSIS

Tests

The model was launched at an angle of approximately 60° with a solid-fuel ABL Deacon rocket booster of about 17,800 lb-sec of total impulse (fig. 2(c)). Separation of the booster-model combination occurred at booster burnout by reason of the drag-weight ratio difference of the model and booster. For use in comparing the aeroelastic properties of the wing in the present investigation with results from other sources, the values of free-stream static pressure obtained during the flight divided by standard sea-level pressure are presented in figure 6 as a function of Mach number. The Reynolds number range of the tests is presented in figure 7.

Analysis

The response of the model to deflections of an all-movable longitudinal control surface in an approximate square-wave program was analyzed by the method of reference 1. A small correction for rate of pitch was applied to the indicated angles of attack to convert them to angles of attack at the center of gravity of the model, reference 10. The wing normal-force measurements were corrected for inertia effects by the method of reference 3.

ACCURACY

The absolute accuracy of the measured quantities in such an investigation cannot be precisely stated. An indication of the systematic instrument errors possible is given by the following table, based on an accuracy of ±1 percent of the full instrument range:

M	C_{N_A}	C_C	C_{N_W}
1.2	±0.009	±0.001	±0.003
1.0	±.013	±.002	±.005
.8	±.022	±.003	±.008

The Mach numbers are accurate to ±1 percent at supersonic speeds and ±2 percent at subsonic speeds. For data presented at an average Mach number during an oscillation, the Mach number varied ±0.01. Further errors in the aerodynamic coefficients may arise from possible dynamic-pressure inaccuracies which are approximately twice as great as errors in Mach number.

Errors in measured angle of attack and control-surface deflection are independent of dynamic pressure and are not likely to vary with Mach number. The control-surface deflections are estimated to be accurate to $\pm 0.1^{\circ}$ and the angle of attack to $\pm 0.2^{\circ}$. An indication of random errors encountered may be noted from the scatter of data points in the plots of coefficients presented herein.

RESULTS AND DISCUSSION

Time History

A time history of some of the data obtained in the present investigation is presented in figure 8. The quantities presented are Mach number, control deflection, angle of attack, and lift coefficient. Model-booster separation occurred at 3.3 seconds with the control surfaces against the -3.5° stop. The difference in trim of the model booster and the model alone caused the model to pitch to a maximum angle of attack of about 6° at separation. As the model pitched during coasting flight, a very small oscillation in control position was indicated (fig. 3). Static tests showed that this variation in control position resulted from bending of the control surfaces in their bearings rather than rotation about the hinge line. Thus for the purpose of analysis the control surfaces were assumed to vary in a square-wave pattern between 0.1° and -3.5° in the free-stream direction throughout the flight (fig. 8).

The low-lift oscillations were generally regular in nature, having fairly constant values of period and trim throughout the oscillation (fig. 8). Nonlinear characteristics of the configuration were indicated during the high-lift oscillations by changing values of period and trim with amplitude. Oscillation 3 (fig. 8) shows the trim-lift-coefficient line drawn through the oscillation. The shaded portion of the lift-coefficient plot denotes an envelope faired through the maximum amplitude of an oscillation imposed on the normal-accelerometer trace which corresponded to the first-bending frequency of the wing. Data below a Mach number of about 0.65 were not analyzed because of the increasing inaccuracy of the instruments at the low dynamic pressures.

Buffeting

A plot of the lift coefficient at constant angle of attack against Mach number is presented in figure 9. The shaded area indicates the lift coefficient at which an oscillation of the wing first-bending frequency was imposed on the normal-accelerometer and wing-balance traces. This boundary was arbitrarily determined from points where the amplitude of the oscillation imposed on the normal-accelerometer trace first reached a value of $\Delta C_{N_A} = \pm 0.015$.

Lift

The experimental lift coefficients of the complete configuration are presented in figure 10 as a function of angle of attack for each oscillation used in the analysis of these data. A similar plot for the wing-alone lift coefficients as obtained from wing-balance data is shown

in figure 11. Average lift-curve slopes of the complete configuration and of the wing alone at $C_L \approx 0$ are plotted against Mach number in figure 12(a) and 12(b), respectively. Calculated rigid values for model lift-curve slope are shown as a dashed line in figure 12(a). The lift-curve slopes for the complete configuration had a maximum value of 0.085 which occurred near $M = 0.95$. For the wing alone the maximum value was about 0.069 near $M = 1.0$. The lift-curve slopes decreased with increasing angles of attack. Throughout the Mach number range investigated the wing accounted for about 80 percent of the total lift.

Drag

Drag variation with lift is shown in figure 13. The minimum drag coefficients of the complete model shown in figure 14, plotted against Mach number, show the same general variation as data from models with similar wings in reference 11. The plot of dC_D/dC_L^2 against Mach number, figure 15, discloses a moderate amount of leading-edge suction throughout the Mach number range covered. The C_L range over which the values of dC_D/dC_L^2 were obtained was about 0 to 0.2 for the low-lift oscillation ($\delta = 0.1^\circ$) and from about 0.2 to 0.3 for the high-lift oscillation ($\delta = -3.5^\circ$). The maximum lift-drag ratios as a function of Mach number (fig. 16) show a maximum value of about 11.0 at high subsonic speeds and about one-half this value at low supersonic speeds. The lift coefficients at which the maximum lift-drag ratios occur are shown in figure 17 plotted against Mach number. The extrapolation indicated by the dashed line of figures 16 and 17 was made by assuming that dC_D/dC_L^2 remains constant up to the value of C_L for $(L/D)_{max}$.

Static Stability

The measured periods plotted against Mach number are shown in figure 18 and illustrate nonlinearity by the variation of period with amplitude over each oscillation, as in reference 12. The lower values of period which occurred at amplitudes of angle of attack less than $\pm 1^\circ$ were used in the manner of reference 1 for determining average slopes of the pitching-moment curves presented in figure 19.

Total pitching-moment coefficients were determined from values of pitching acceleration found using values of normal force at the center of gravity and angle of attack in a double-differentiation process as in reference 8. The variation of the pitching-moment coefficient with lift coefficient is shown in figure 20 with slopes from the period method (fig. 19) drawn through values of trim lift coefficient at $C_m = 0$.

Previous models with 45° swept wings of aspect ratio 4.0 and a tail mounted 0.50 wing semispans above the model center line showed considerable pitch-up tendencies in the high subsonic Mach number range at high-lift coefficients, references 8 and 13. Data from tests on the same $A = 4$ plan-form wing with a different fuselage and without a tail also showed the pitch-up characteristics, reference 14. Bump tests of a wing configuration identical to that of the present investigation showed considerable pitch-up characteristics, reference 15. For the model flown in this investigation no pitch-up was encountered. This is probably due to the low tail position of the present investigation. Beneficial effects of low tail position for a configuration similar to that of the present investigation are indicated in reference 16.

For the complete configuration a rearward movement of the aerodynamic center from 45 percent of the wing mean aerodynamic chord at subsonic speeds to about 85 percent at low supersonic speeds is noted in figure 21. Also shown in figure 21 are values converted to rigid-wing conditions by the method of reference 8 for a 0.25-chord loading. A 10-percent wing-mean-aerodynamic-chord forward movement of the aerodynamic center is occasioned by an inboard movement of the wing load due to flexibility.

Damping in Pitch

Time for the oscillation in pitch to damp to one-half amplitude is plotted against Mach number in figure 22(a) and converted to the rotary damping factor $C_{m_q} + C_{m_{\dot{\alpha}}}$ plotted against Mach number in figure 22(b). The loss in damping near Mach number 1.0 was found for models with a similar wing (figs. 3 and 4 of ref. 17). A comparison with calculated values up to $M = 0.9$, figure 22(b), for wing-plus-tail from reference 17 shows good agreement with the experimental values in the present investigation. The C_{L_α} term of the pitch damping factor (ref. 17) contributed about one-half of the total damping.

Longitudinal Trim

Values of trim lift coefficient obtained from the time-history plots for two control positions and calculated values of lift coefficient required for level flight at 40,000 feet with a wing loading of 80 lb/sq ft are shown in figure 23(a) plotted against Mach number. An indication of control deflection required for level flight under the given conditions may be observed from figure 23(a).

In previous high-tail models, reference 2, a change in trim for tail deflections near zero of about 1° occurred at high subsonic Mach numbers and was attributed to the flow over the converging rear portion

of the fuselage. With the control surfaces mounted normal to the fuselage in the low position of the present investigation, no abrupt changes in trim were observed for the low tail deflection. Trim-angle-of-attack variation with Mach number is shown in figure 23(b). For the high lift control position the greatest change in trim occurred between $M = 0.90$ to $M = 1.0$.

CONCLUSIONS

Analysis of the data obtained in the present investigation and comparison with results from closely similar investigations indicate the following conclusions:

1. The lift-curve slope of the model had a maximum value of 0.085 which occurred near $M = 0.95$. For the wing alone the maximum value was about 0.069 near $M = 1.0$. Throughout the Mach number range investigated the wing accounted for about 80 percent of the total lift.

2. The minimum-drag curve of the complete model showed a drag rise beginning at about $M = 0.95$. The minimum drag had not reached a maximum value at the highest Mach number obtained ($M = 1.21$).

3. An indication of a moderate value of leading-edge suction was obtained throughout the Mach number range investigated.

4. Experimental maximum lift-drag ratios averaging about 11.0 were obtained at high subsonic speeds. Maximum lift-drag ratios of about 5.0 were calculated from the low lift experimental data at low supersonic speeds.

5. No pitch-up was experienced by the low tail configuration of the present investigation up to $C_L = 0.85$ at $M = 0.75$.

6. The aerodynamic center moved rearward from about 45 percent of the mean aerodynamic chord at high subsonic speeds to about 85 percent at low supersonic speeds.

7. The pitch damping factor $C_{m_q} + C_{m_{\dot{\alpha}}}$ was a minimum near $M = 1.0$.

Langley Aeronautical Laboratory,
National Advisory Committee for Aeronautics,
Langley Field, Va., July 30, 1953.

REFERENCES

1. Gillis, Clarence L., Peck, Robert F., and Vitale, A. James: Preliminary Results From a Free-Flight Investigation at Transonic and Supersonic Speeds of the Longitudinal Stability and Control Characteristics of an Airplane Configuration with a Thin Straight Wing of Aspect Ratio 3. NACA RM L9K25a, 1950.

2. Gillis, Clarence L., and Vitale, A. James: Wing-On and Wing-Off Longitudinal Characteristics of an Airplane Configuration Having a Thin Unswept Tapered Wing of Aspect Ratio 3, As Obtained From Rocket-Propelled Models at Mach Numbers from 0.8 to 1.4. NACA RM L50K16, 1951.

3. Vitale, A. James, McFall, John C., Jr., and Morrow, John D.: Longitudinal Stability and Drag Characteristics at Mach Numbers From 0.75 to 1.5 of an Airplane Configuration Having a 60° Swept Wing of Aspect Ratio 2.24 As Obtained From Rocket-Propelled Models. NACA RM L51K06, 1952.

4. Parks, James H.: Longitudinal Aerodynamic Characteristics of a Model Airplane Configuration Equipped With a Scaled X-1 Airplane Wing. NACA RM L51L10a, 1952.

5. Chapman, Rowe, Jr., and Morrow, John D.: Longitudinal Stability and Drag Characteristics at Mach Numbers From 0.70 to 1.37 of Rocket-Propelled Models Having a Modified Triangular Wing. NACA RM L52A31, 1952.

6. McFall, John C., Jr., and Hollinger, James A.: Longitudinal Stability, Control Effectiveness, and Drag Characteristics at Transonic Speeds of a Rocket-Propelled Model of an Airplane Configuration Having an Unswept Wing of Aspect Ratio 3.0 and NACA 65A004.5 Airfoil Sections. NACA RM L52L04, 1953.

7. Peck, Robert F. and Mitchell, Jesse L.: Rocket-Model Investigation of Longitudinal Stability and Drag Characteristics of an Airplane Configuration Having a 60° Delta Wing and a High Unswept Horizontal Tail. NACA RM L52K04a, 1953.

8. Vitale, A. James: Effects of Wing Elasticity on the Aerodynamic Characteristics of an Airplane Configuration Having 45° Sweptback Wings As Obtained From Free-Flight Rocket-Model Tests at Transonic Speeds. NACA RM L52L30, 1953.

9. Parks, James H., and Kehlet, Alan B.: Longitudinal Stability, Trim, and Drag Characteristics of a Rocket-Propelled Model of an Airplane Configuration Having a 45° Sweptback Wing and an Unswept Horizontal Tail. NACA RM L52F05, 1952.

10. Mitchell, Jesse L., and Peck, Robert F.: An NACA Vane-Type Angle-of-Attack Indicator for Use at Subsonic and Supersonic Speeds. NACA RM L9F28a, 1949.

11. Pepper, William B., Jr., and Hoffman, Sherwood: Transonic Flight Tests To Compare the Zero-Lift Drag of Underslung and Symmetrical Nacelles Varied Chordwise at 40 Percent Semispan of a 45° Sweptback, Tapered Wing. NACA RM L50G17a, 1950.

12. Curfman, Howard J., Jr.: Theoretical and Analog Studies of the Effects of Nonlinear Stability Derivatives on the Longitudinal Motions of an Aircraft in Response to Step Control Deflections and to the Influence of Proportional Automatic Control. NACA RM L50L11, 1951.

13. Donlan, Charles J., and Weil, Joseph: Characteristics of Swept Wings at High Speeds. NACA RM L52A15, 1952.

14. Osborne, Robert S.: A Transonic-Wing Investigation in the Langley 8-Foot High-Speed Tunnel at High Subsonic Mach Numbers and at a Mach Number of 1.2. Wing-Fuselage Configuration Having a Wing of 45° Sweepback, Aspect Ratio 4, Taper Ratio 0.6, and NACA 65A006 Airfoil Section. NACA RM L50H08, 1950.

15. Spreemann, Kenneth P., Morrison, William D., Jr., and Pasteur, Thomas B., Jr.: Aerodynamic Characteristics of a Wing With Quarter-Chord Line Swept Back 45°, Aspect Ratio 6, Taper Ratio 0.6, and NACA 65A009 Airfoil Section. NACA RM L50B03a, 1950.

16. Holdaway, George H.: Comparison of the Aerodynamic Characteristics at Transonic Speeds of a Plane Wing and a Cambered and Twisted Wing, Both Having 45° of Sweepback and an Aspect Ratio of 6. NACA RM A53B16, 1953.

17. Gillis, Clarence L., and Chapman, Rowe, Jr.: Summary of Pitch-Damping Derivatives of Complete Airplane and Missile Configurations As Measured in Flight at Transonic and Supersonic Speeds. NACA RM L52K20, 1953.

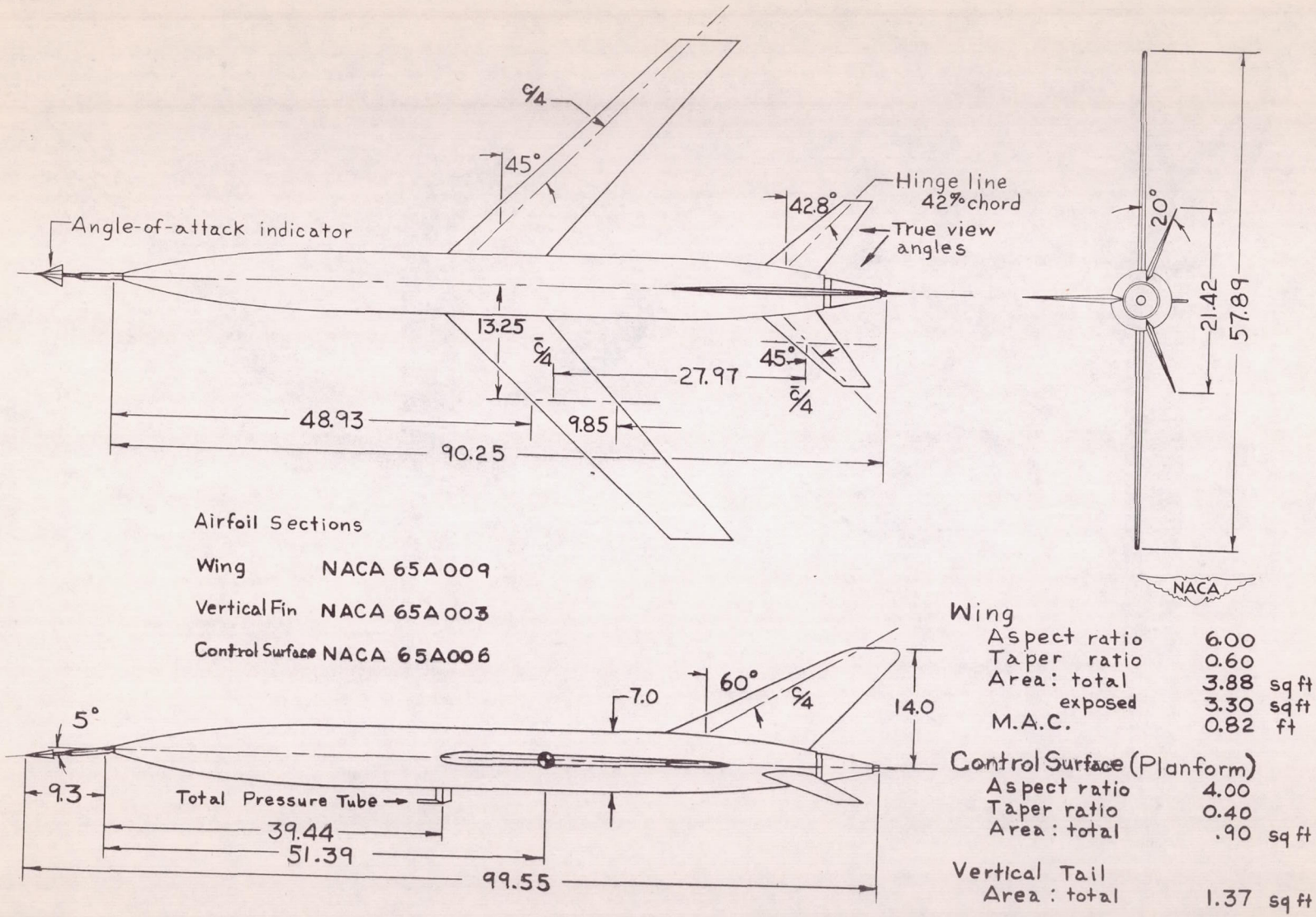

Figure 1.- Physical characteristics of model. All linear dimensions in inches.

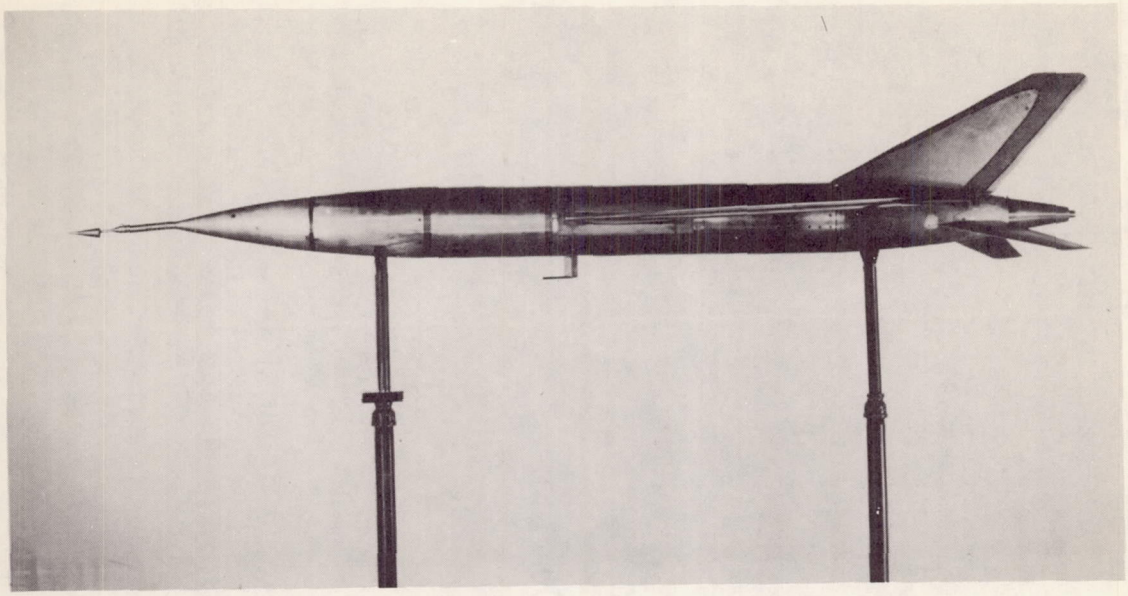

L-75307.1

(a) Side view.

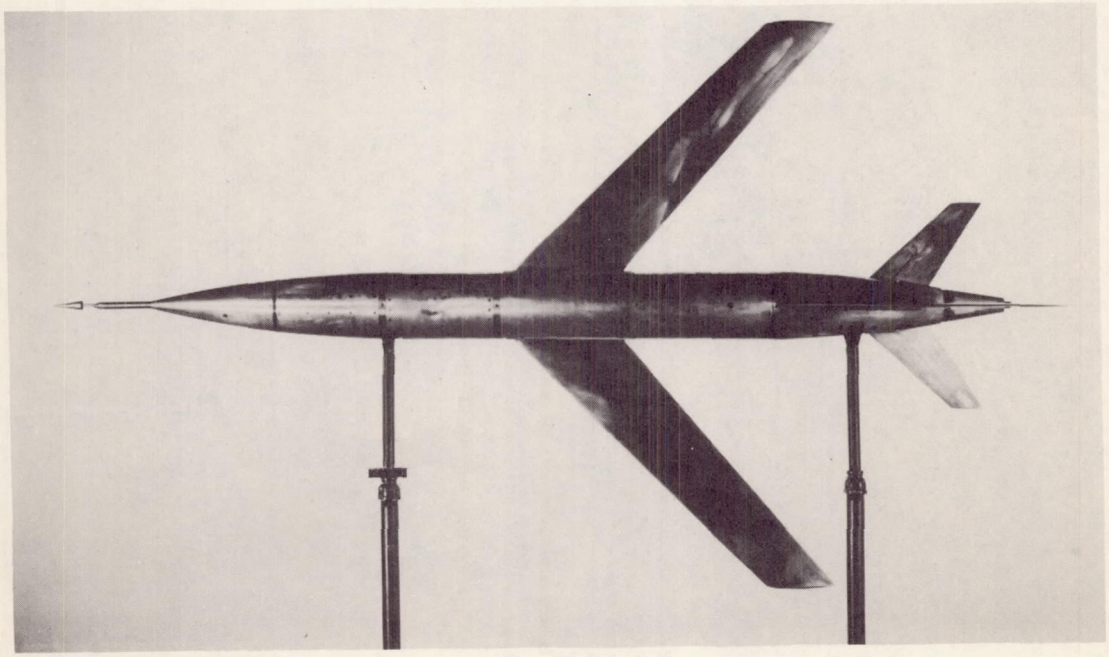

L-75309.1

(b) Top view.

Figure 2.- Photographs of model.

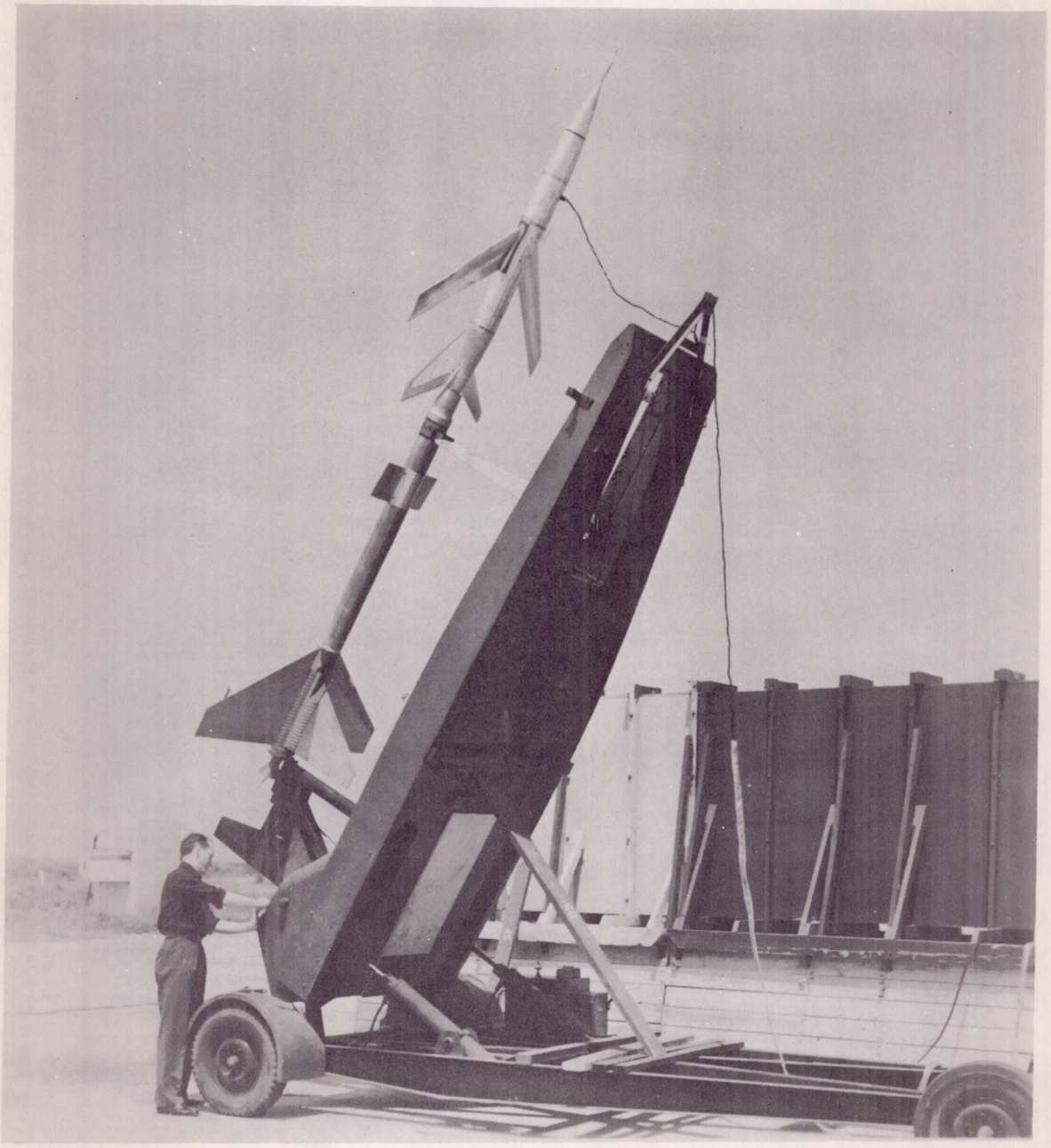

L-75572

(c) Model on launcher.

Figure 2.- Concluded.

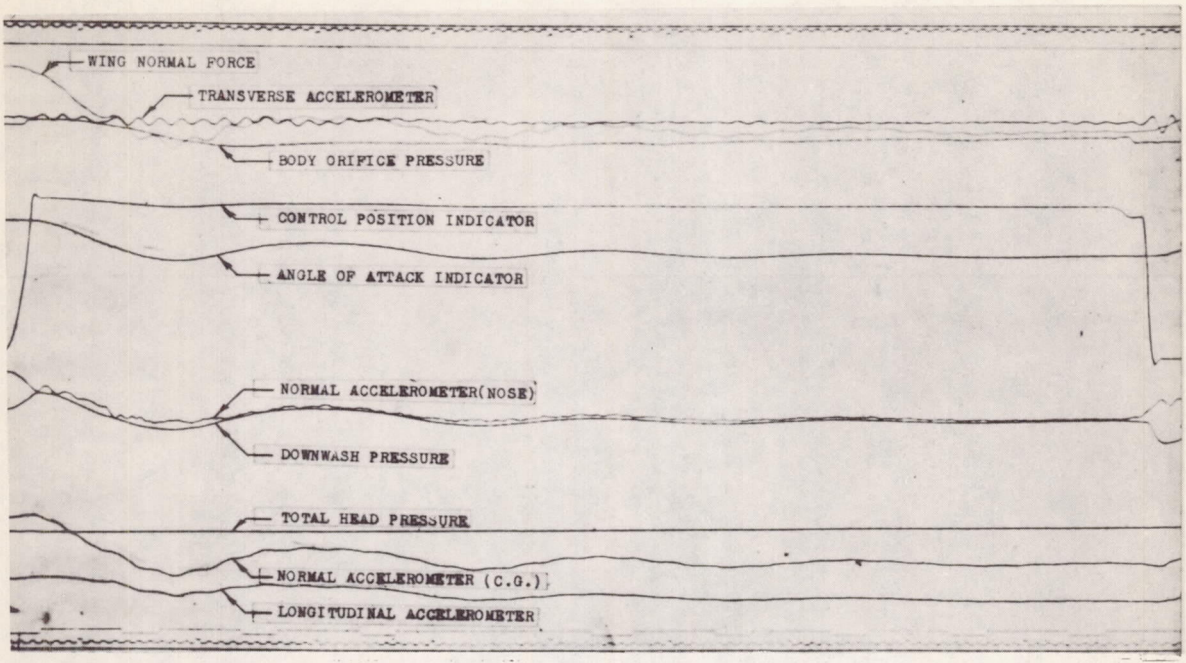

(a) $\delta = -3.5^{\circ}$.

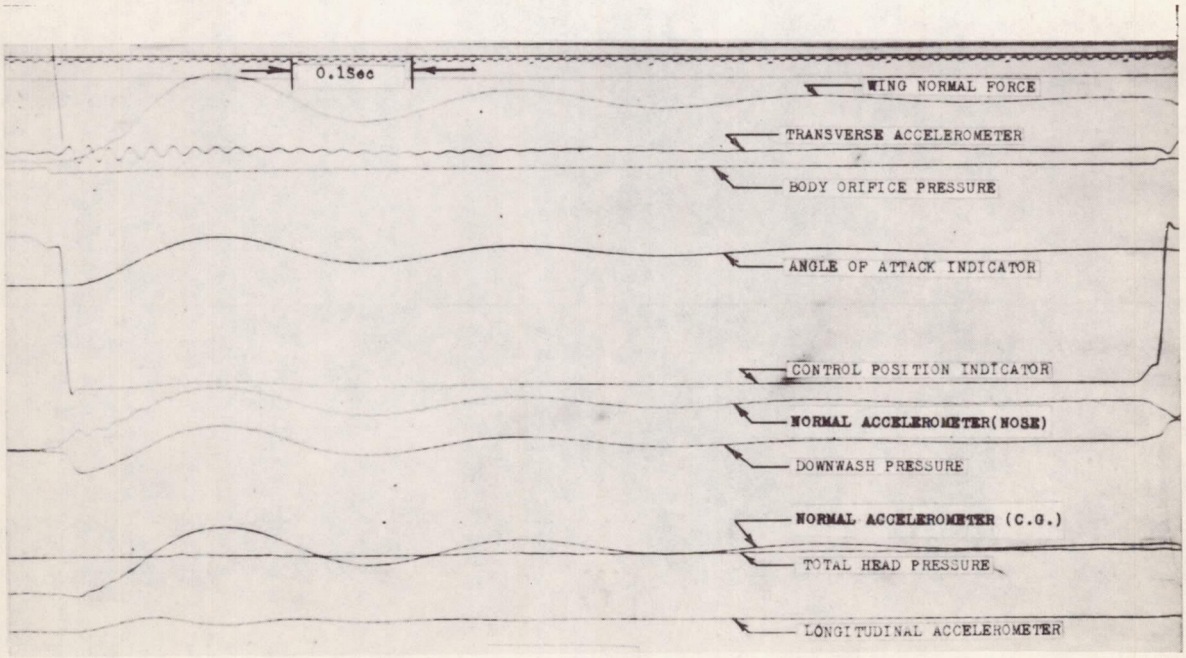

(b) $\delta = 0.1^{\circ}$.

Figure 3.- Section of the telemeter record showing measured quantities of the present investigation.

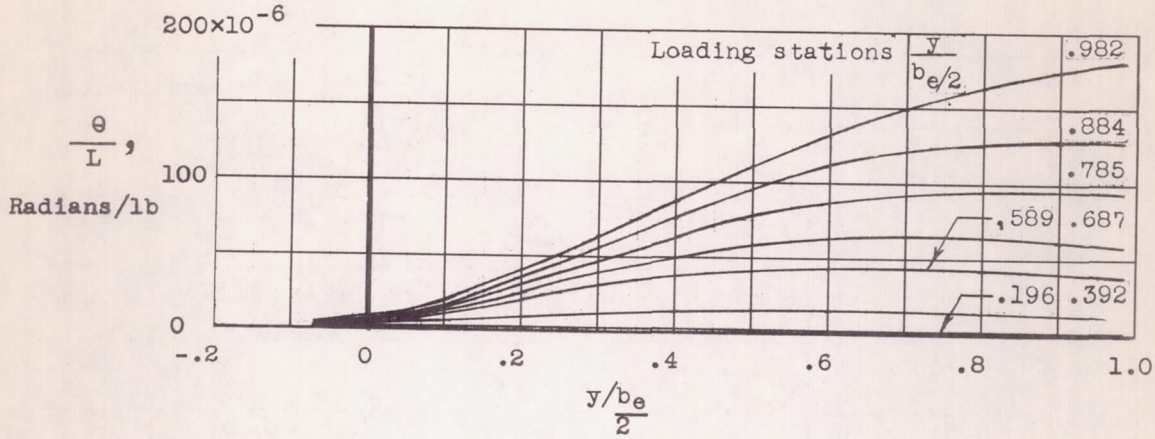

(a) Load applied along 25-percent-chord line.

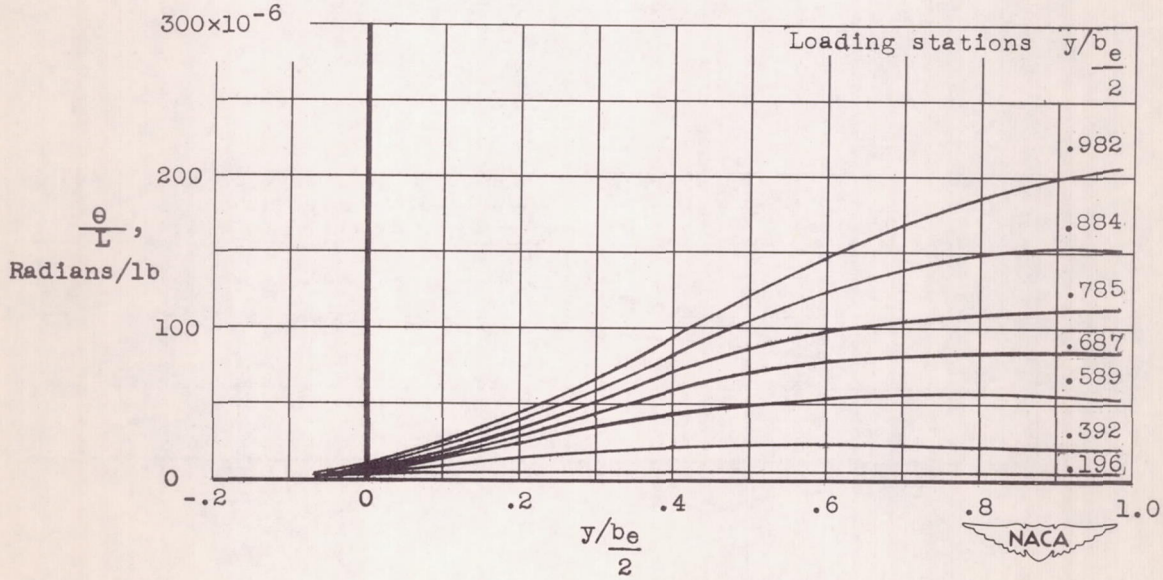

(b) Load applied along 50-percent-chord line.

Figure 4.- Twist in the free-stream direction per unit load applied at various stations along the span of the wing.

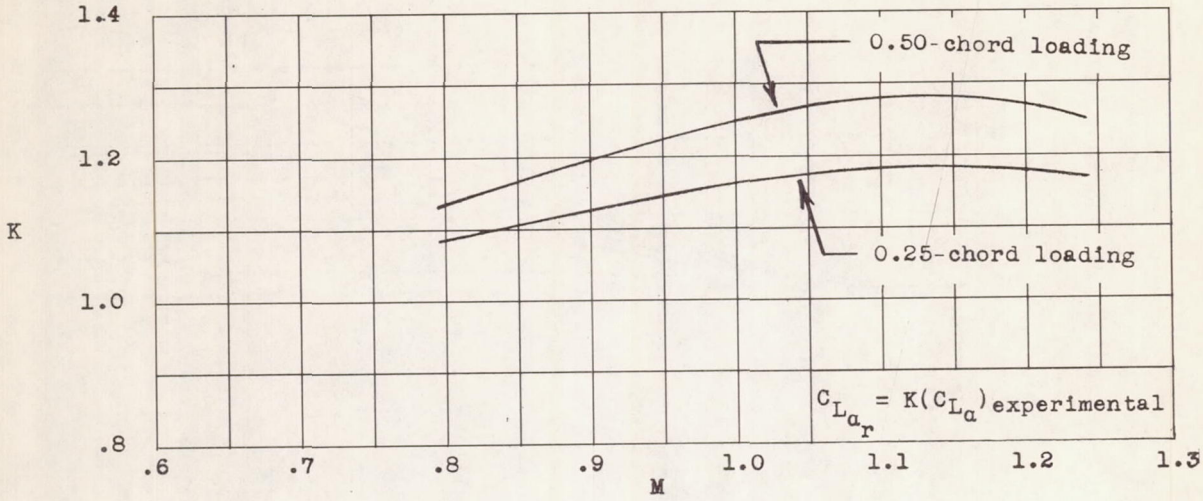

(a) Factor for converting experimental lift-curve slope to rigid conditions.

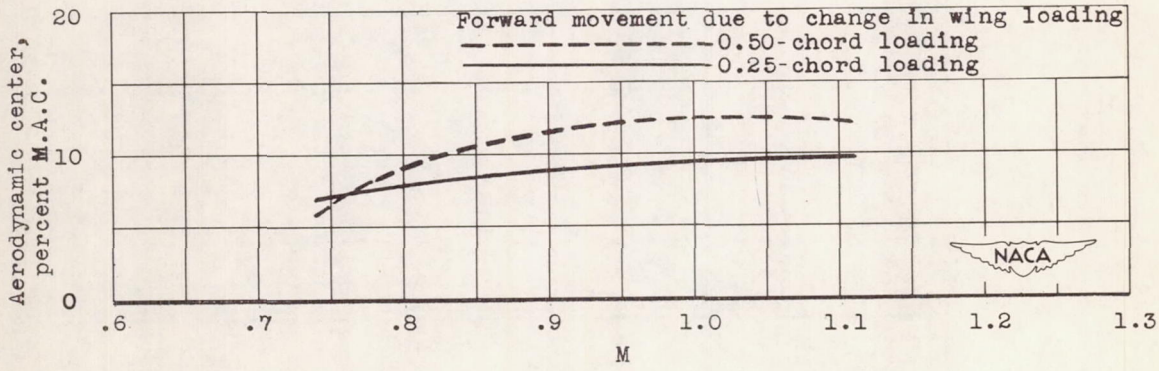

(b) Aerodynamic-center movement.

Figure 5.- Aeroelastic effects.

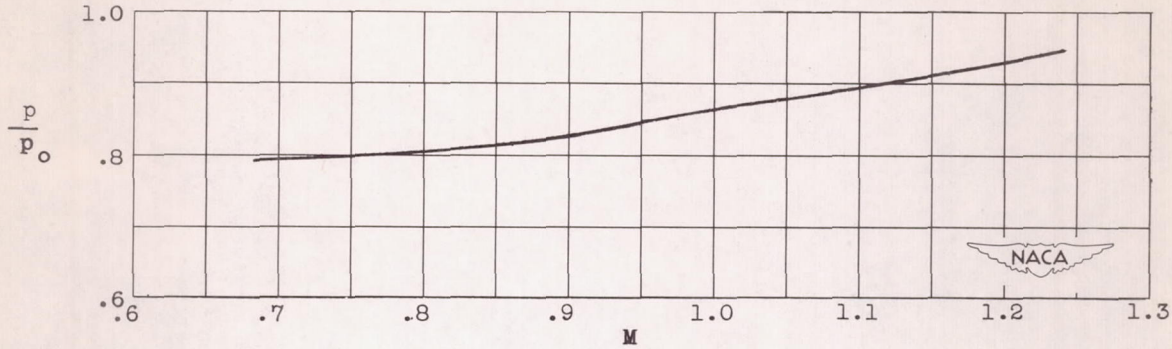

Figure 6.- Static pressure ratio.

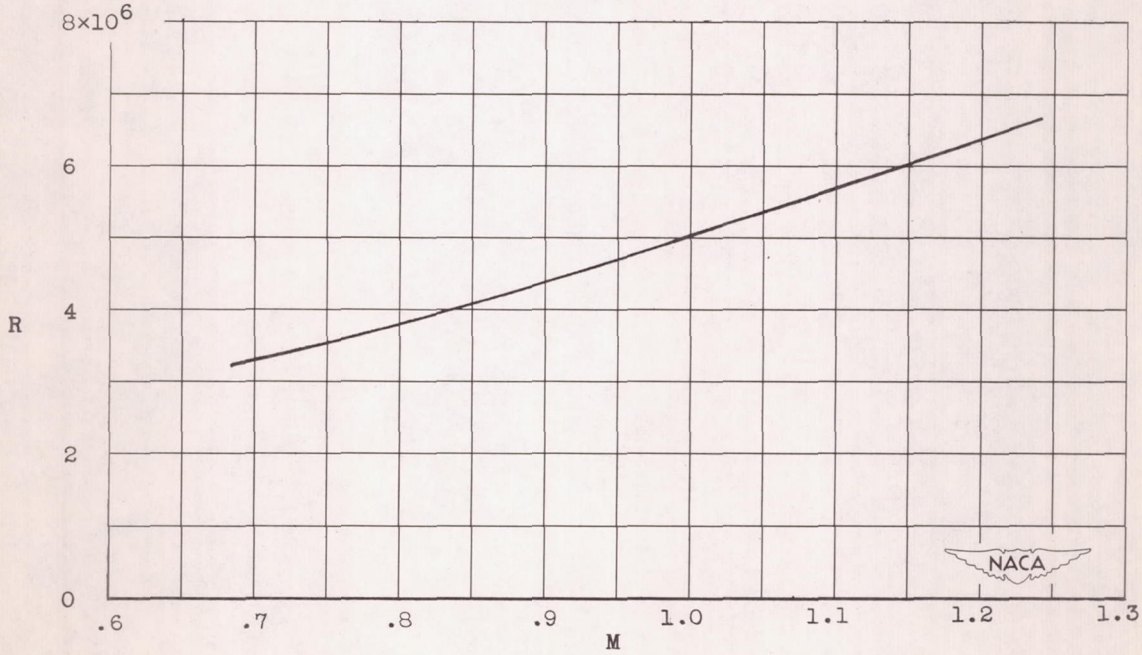

Figure 7.- Reynolds number of test based on wing mean aerodynamic chord.

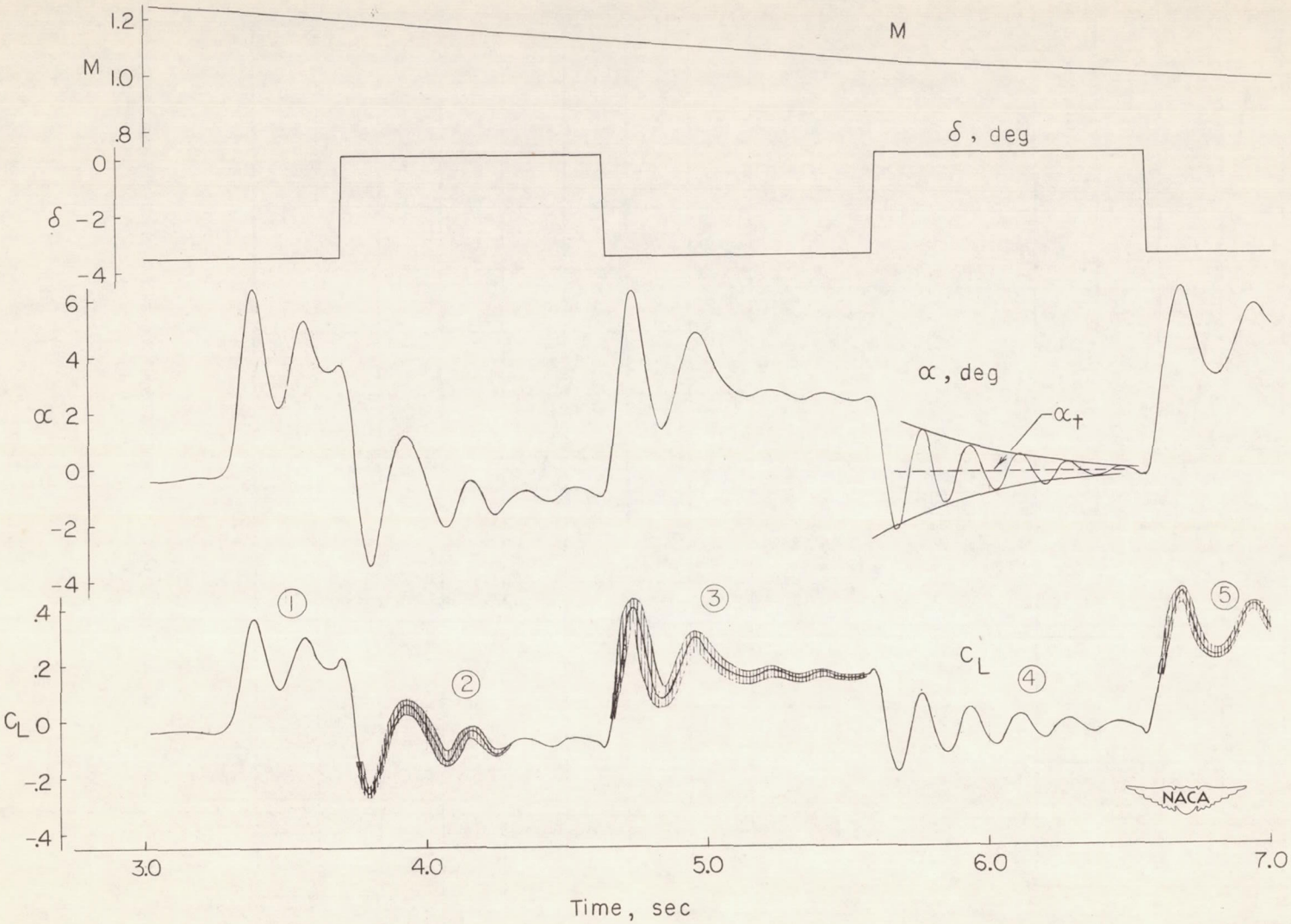

Figure 8.- Time history of some of the quantities in the present investigation.

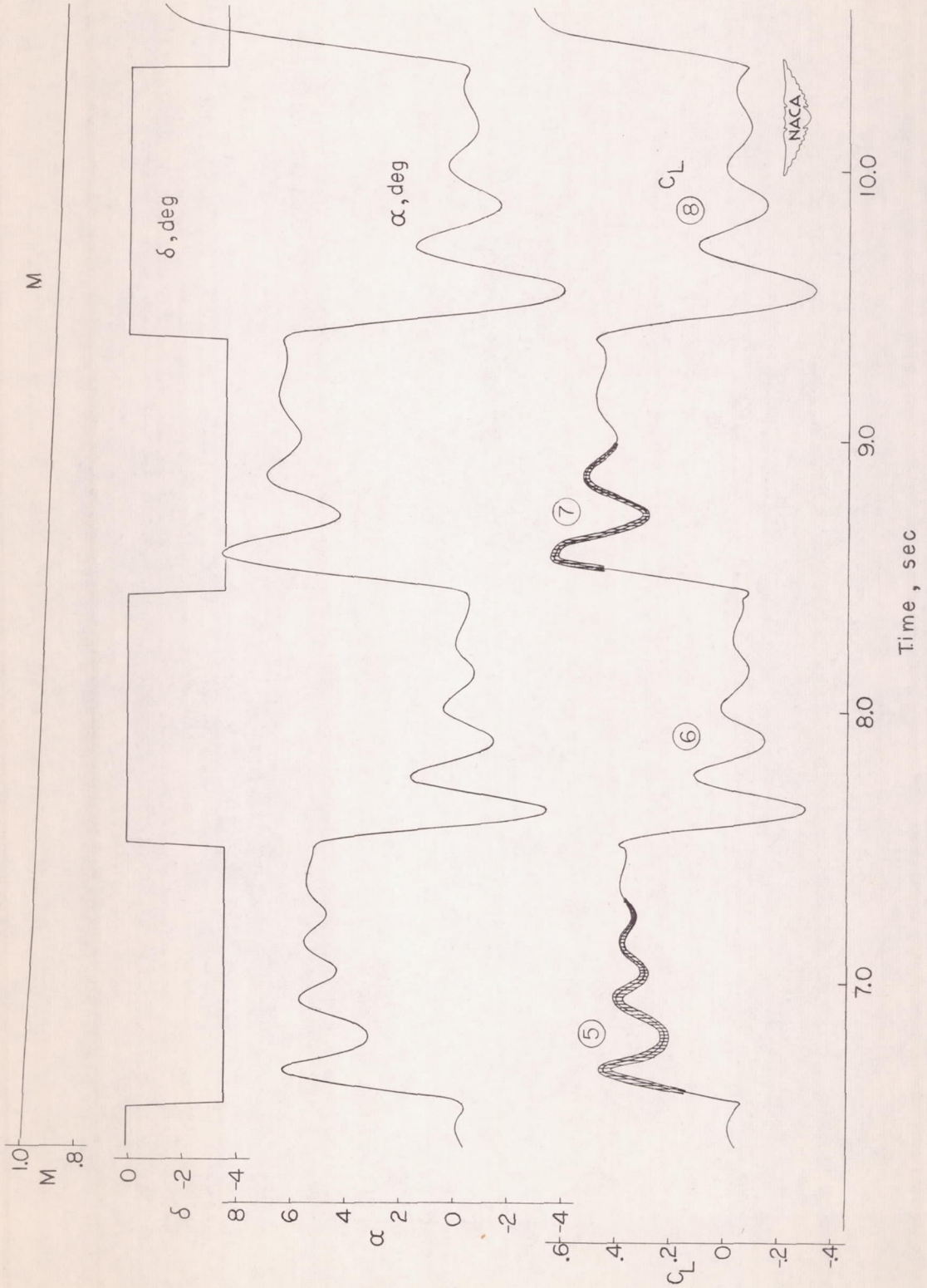

Figure 8.- Continued.

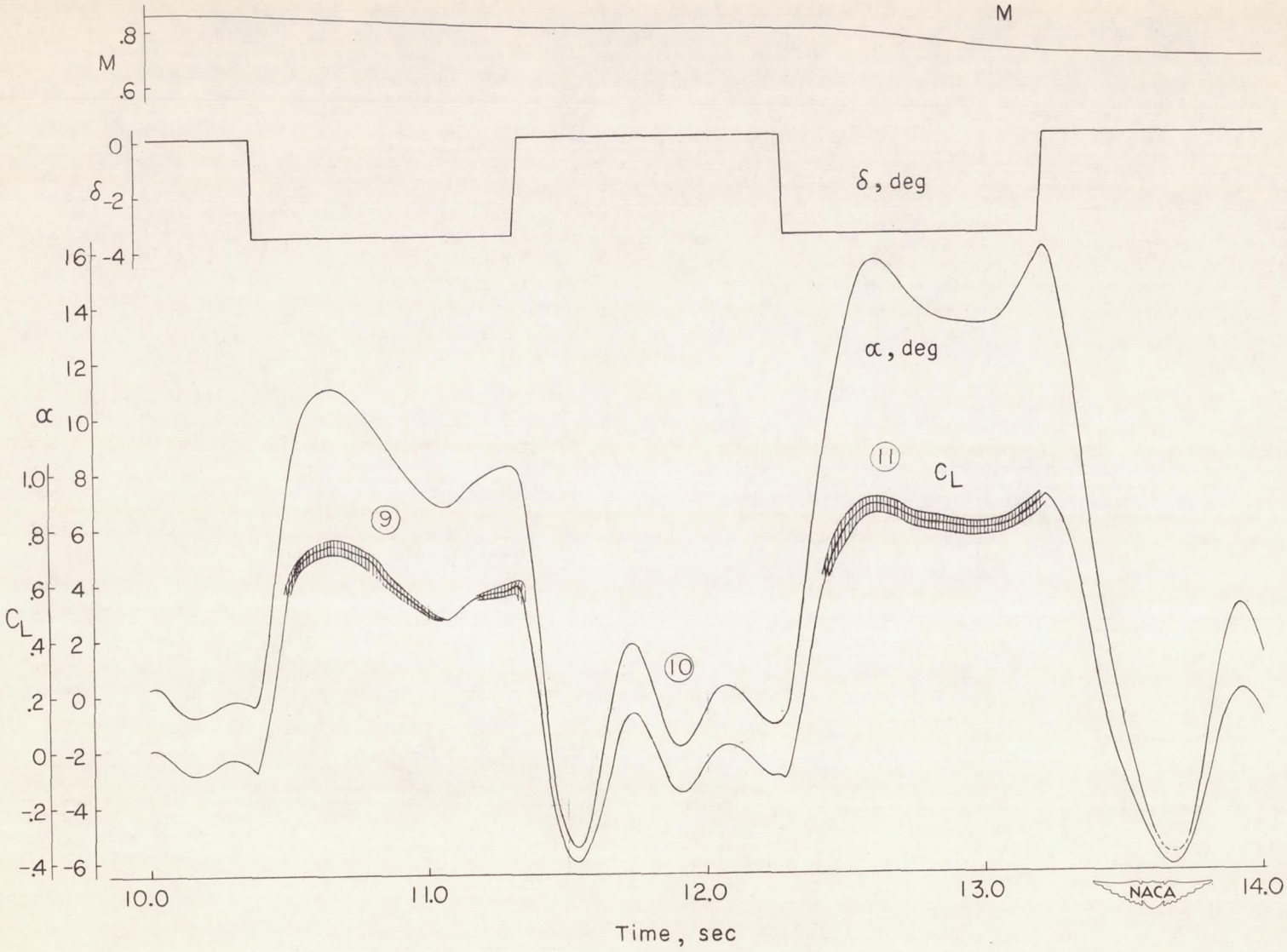

Figure 8.- Concluded.

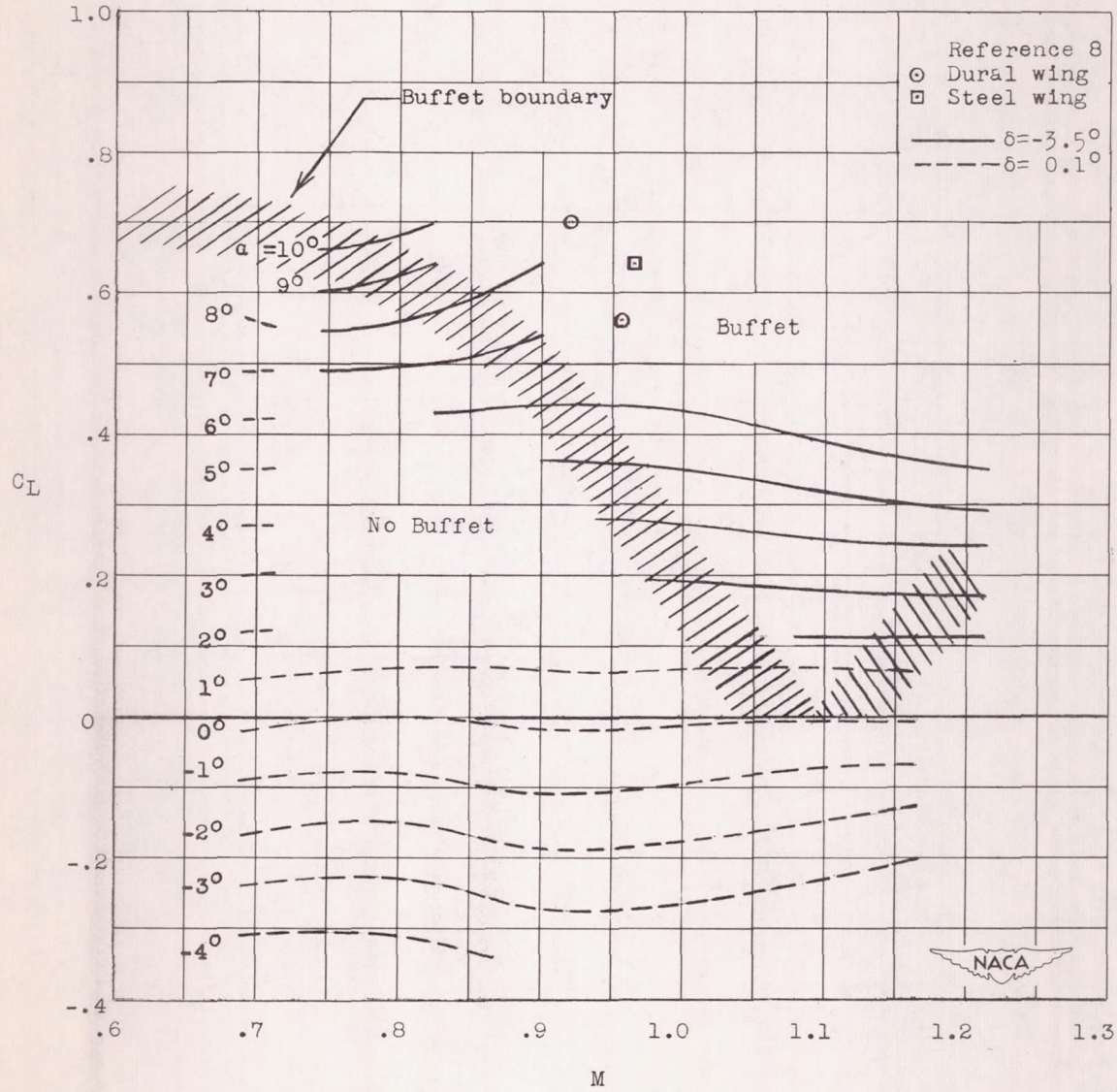

Figure 9.- Lift coefficients for constant angles of attack plotted against Mach number.

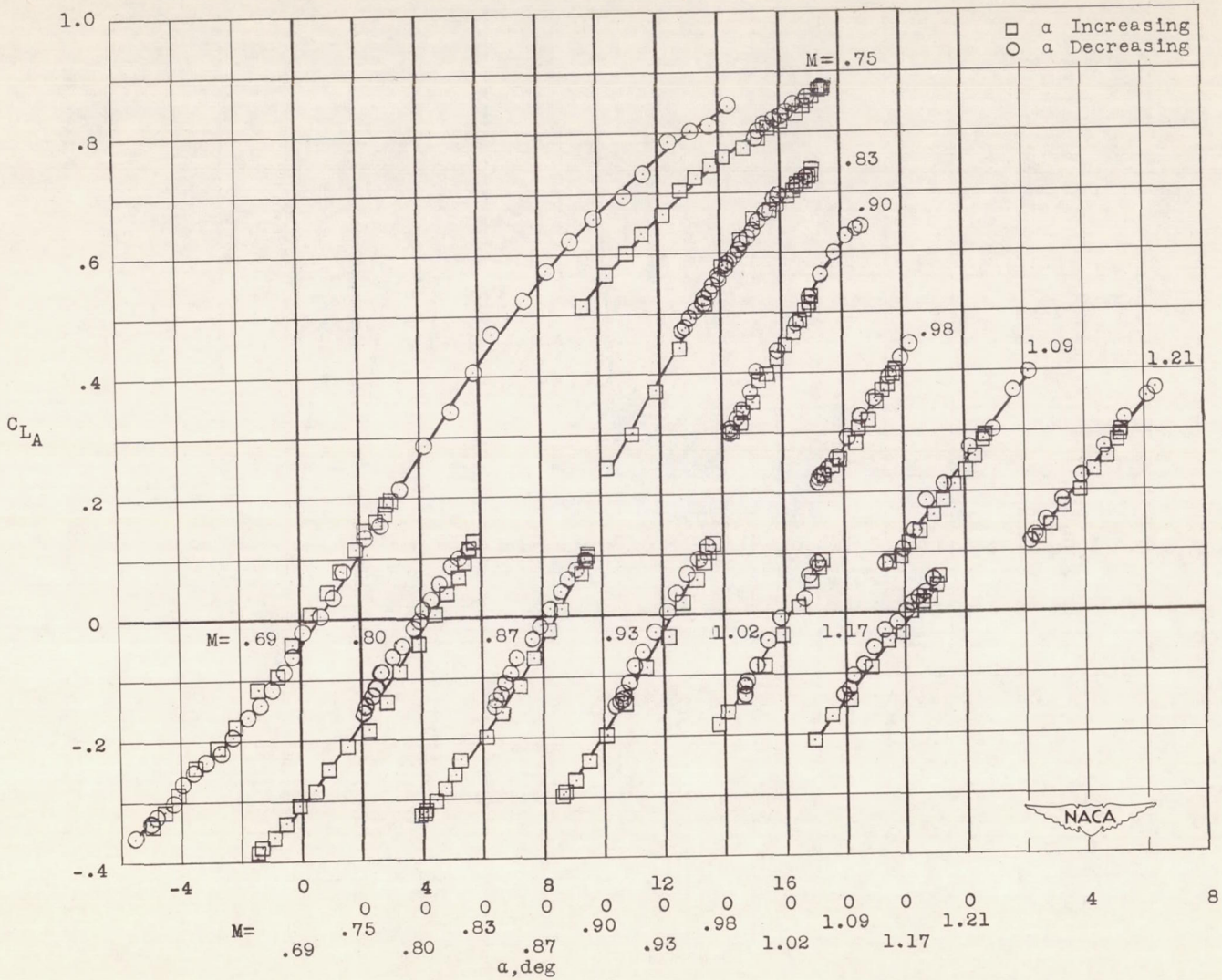

Figure 10.- Variation of model lift coefficient with angle of attack.

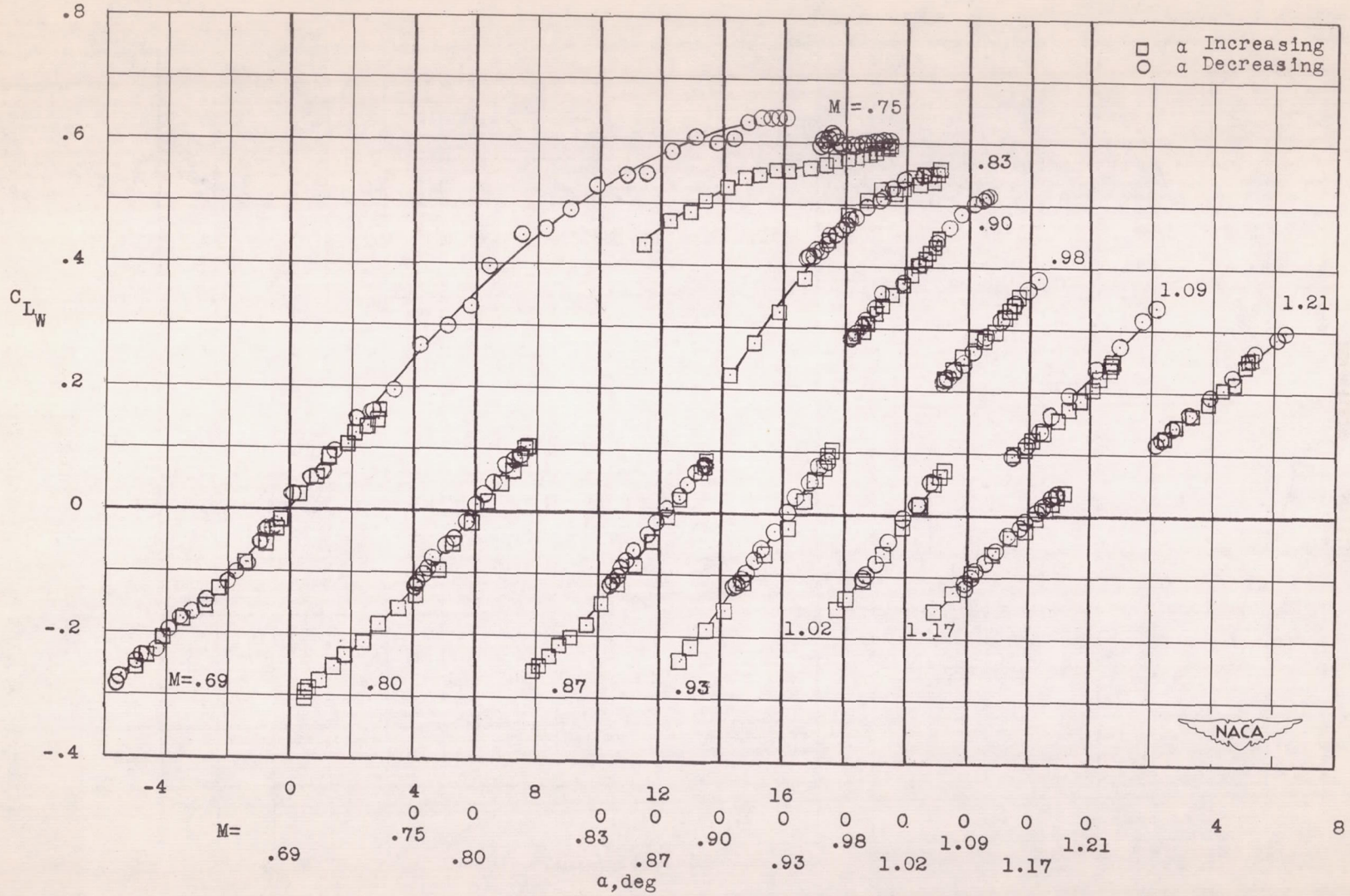

Figure 11.- Variation of wing lift coefficient with angle of attack.

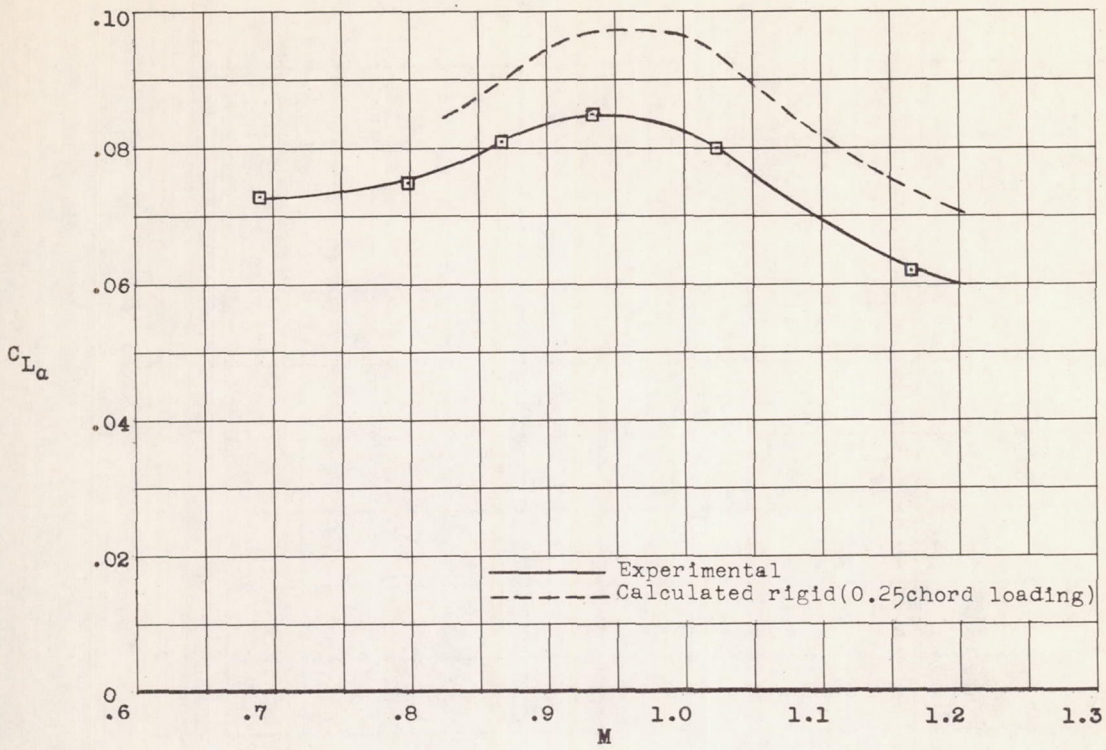

(a) Model.

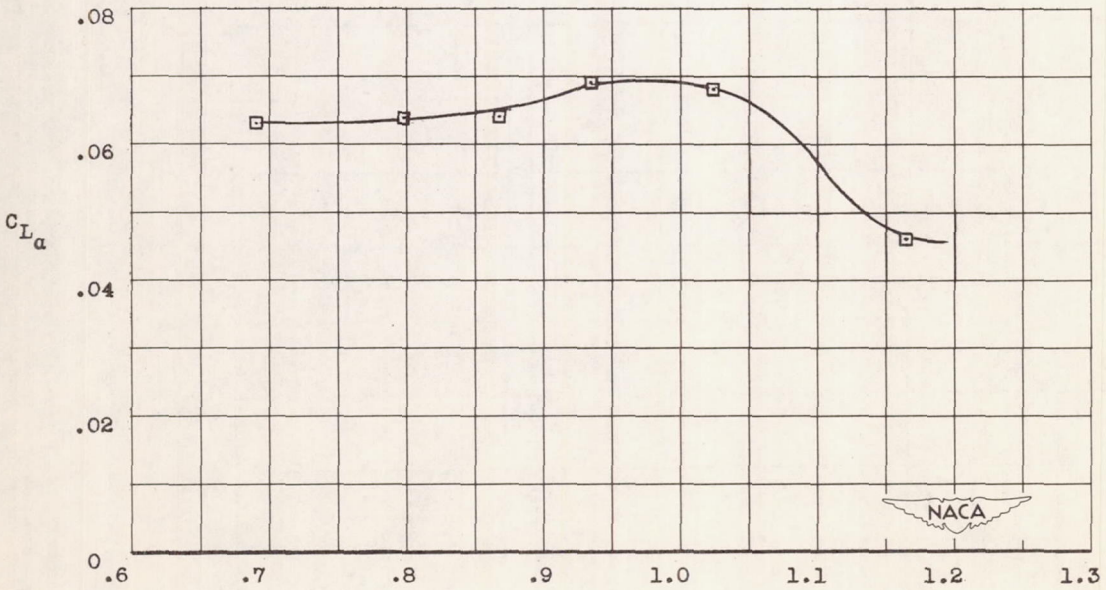

(b) Wing.

Figure 12.- Lift-curve slope for values of $C_L \approx 0$.

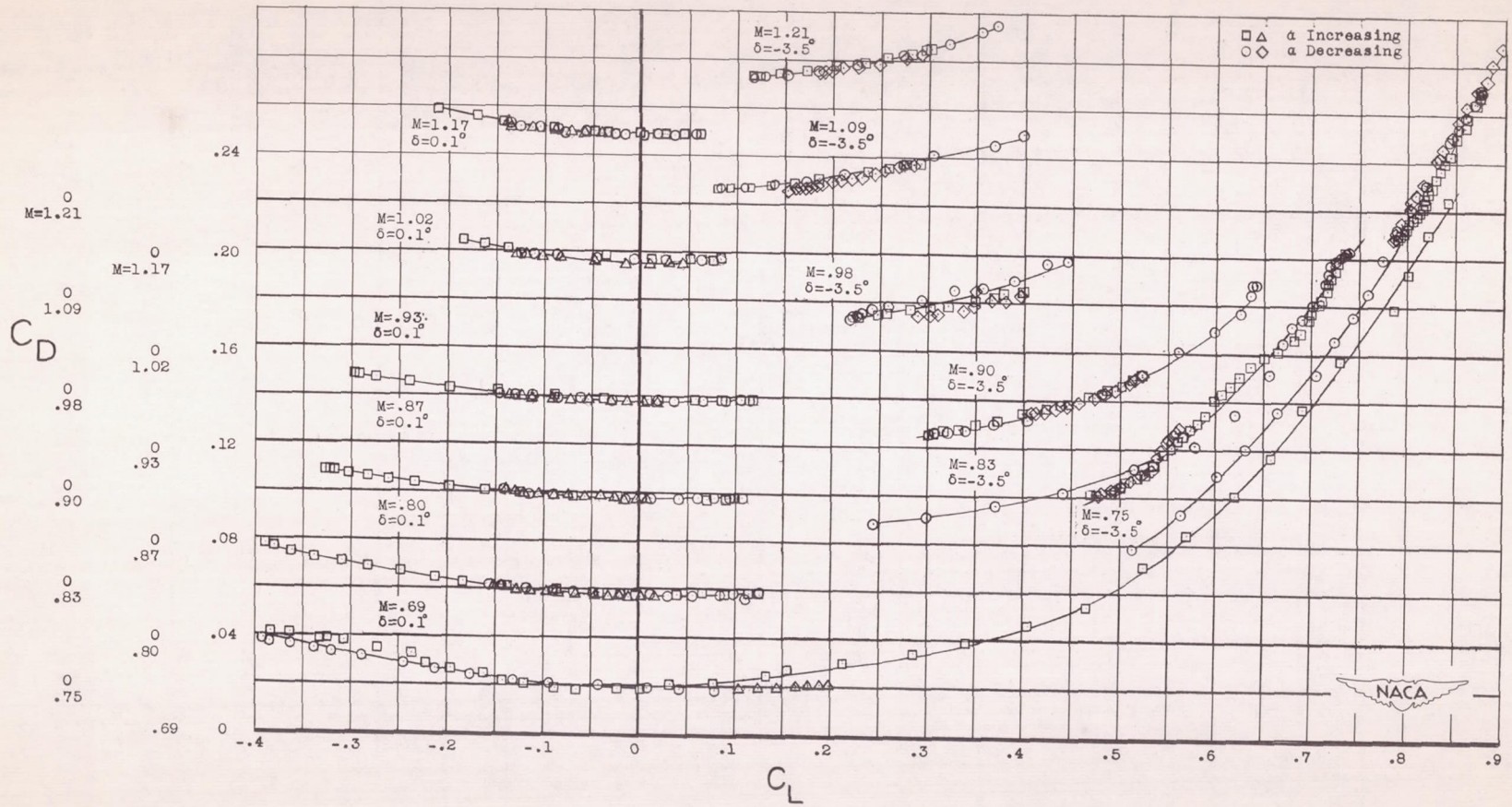

Figure 13.- Variation of drag with lift.

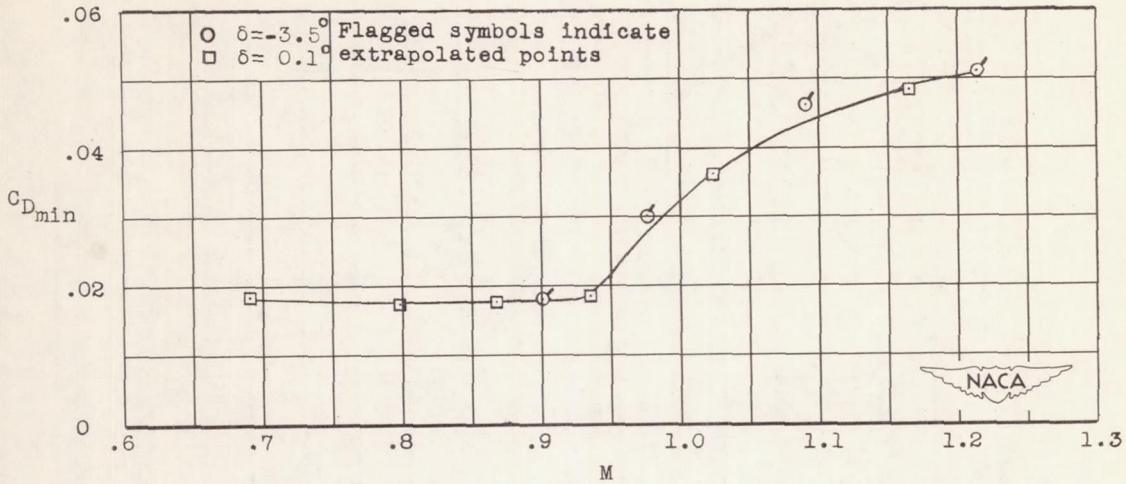

Figure 14.- Minimum drag coefficients of complete model.

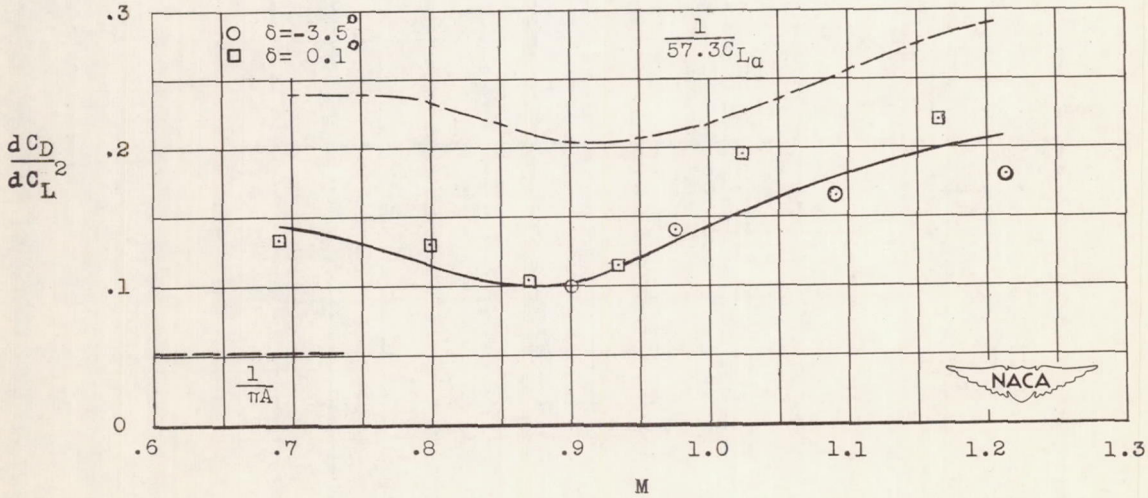

Figure 15.- Effect of lift on drag from values of $C_L \leqq 0.3$.

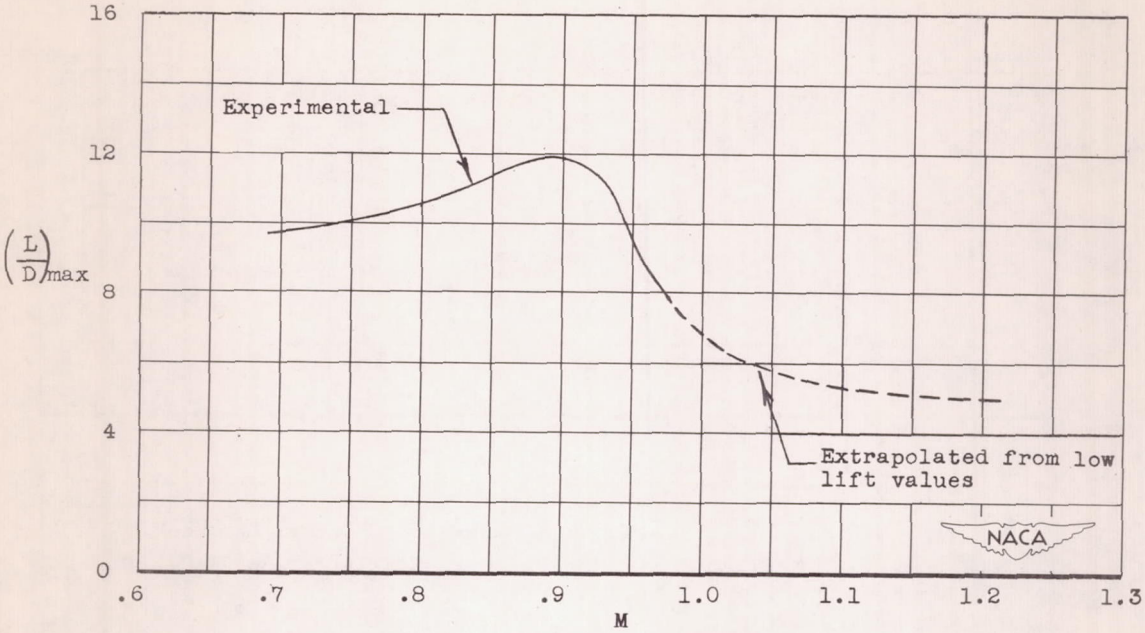

Figure 16.- Maximum lift-drag ratios.

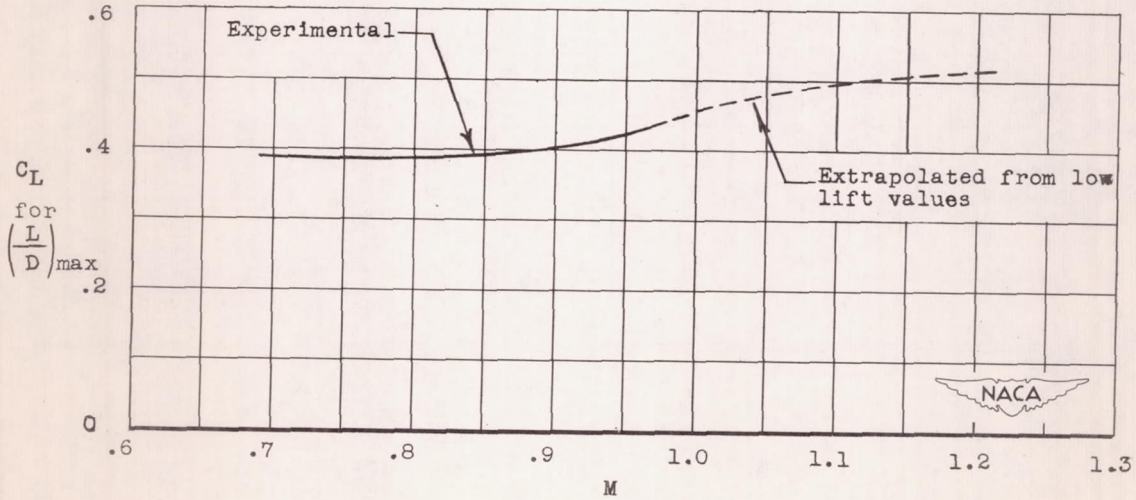

Figure 17.- Lift coefficients for maximum lift-drag ratios.

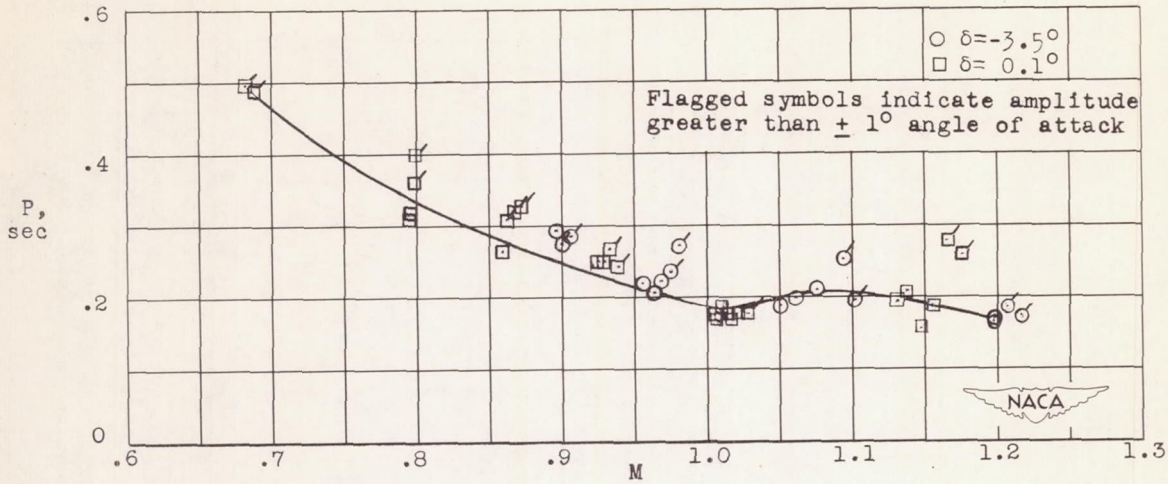

Figure 18.- Measured periods plotted against Mach number illustrating nonlinear characteristics of the configuration by the variation of period with amplitude over each oscillation.

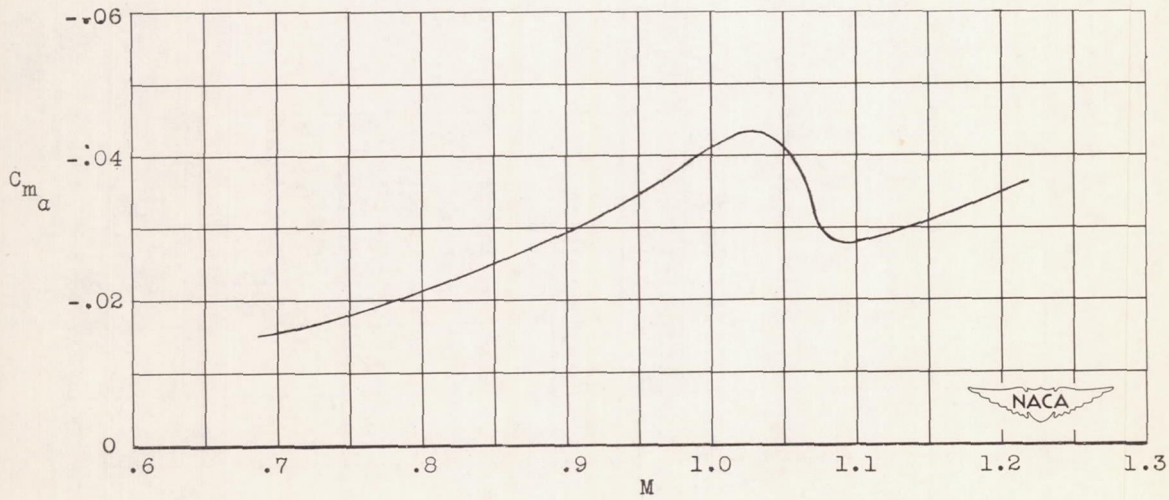

Figure 19.- Slopes of the pitching-moment curves over a range of $|\Delta\alpha| < 1^{\circ}$.

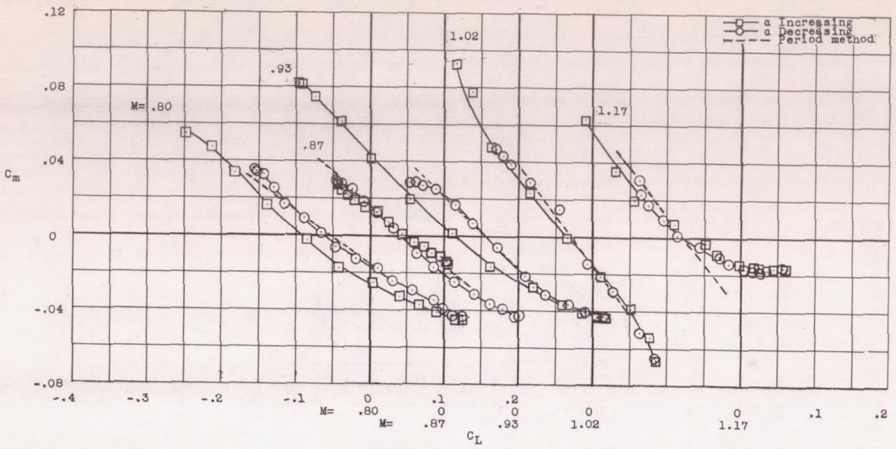

(a) $\delta = 0.1^{\circ}$.

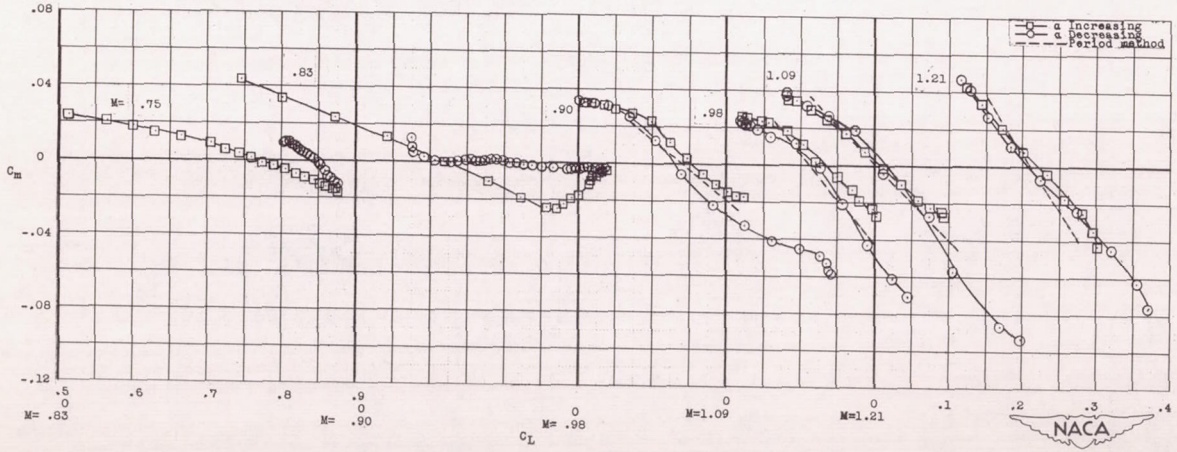

(b) $\delta = -3.5^{\circ}$.

Figure 20.- Variation of pitching-moment coefficient with model lift coefficient.

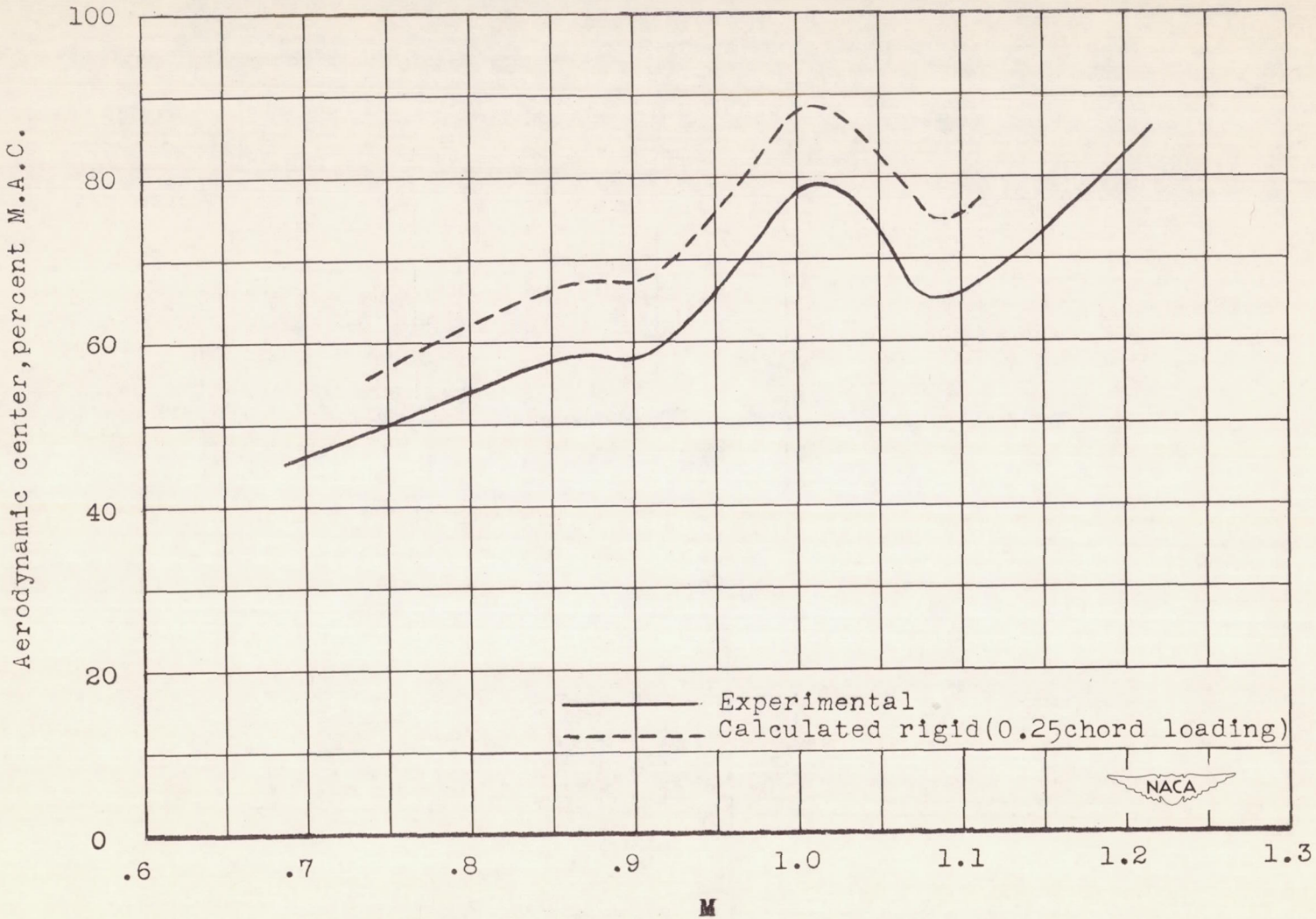

Figure 21.- Variation of aerodynamic center in percent wing mean aerodynamic chord with Mach number for $|\Delta\alpha| < 1^{\circ}$.

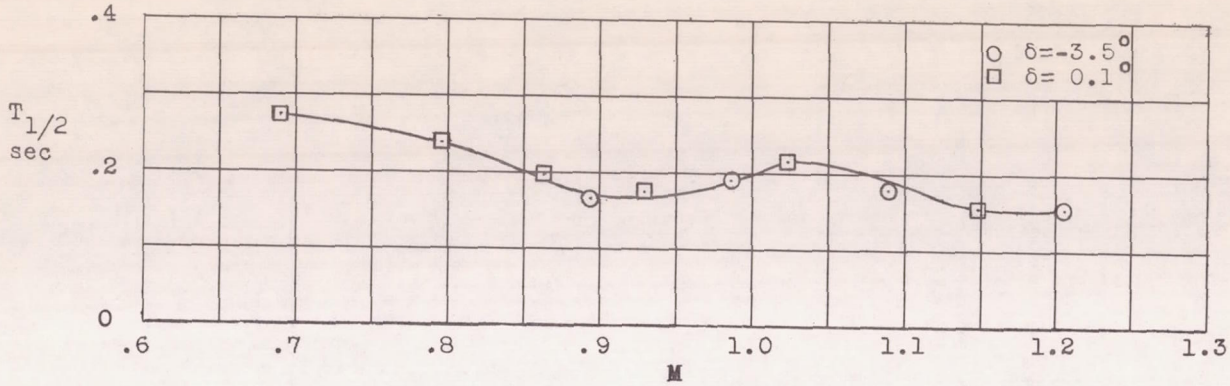

(a) Time to damp to one-half amplitude.

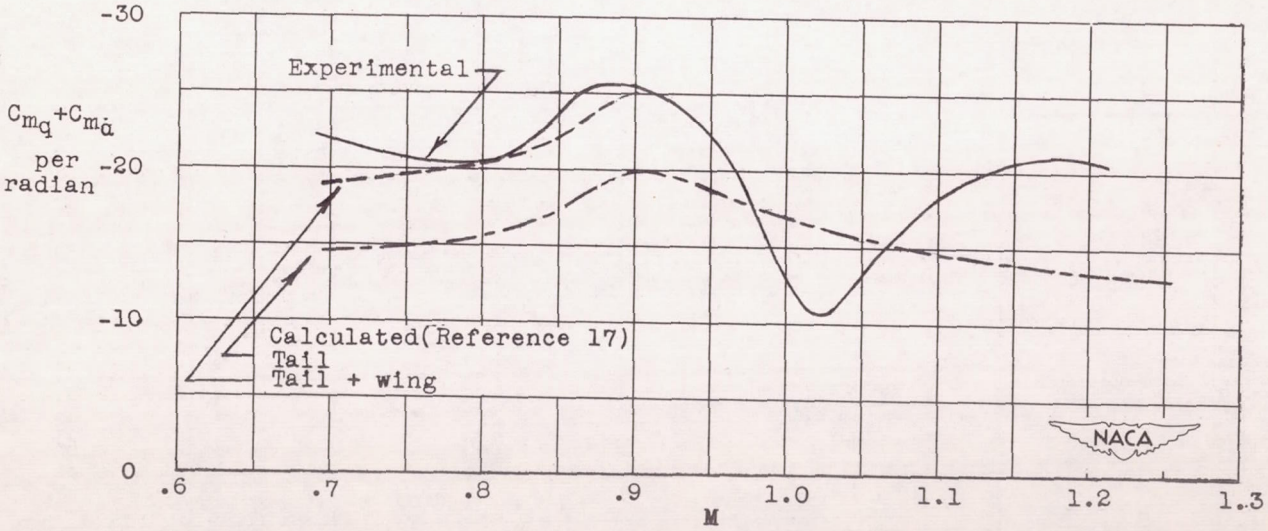

(b) Pitching-moment damping factor $C_{m_q} + C_{m_{\dot{\alpha}}}$.

Figure 22.- Damping characteristics of short-period oscillations.

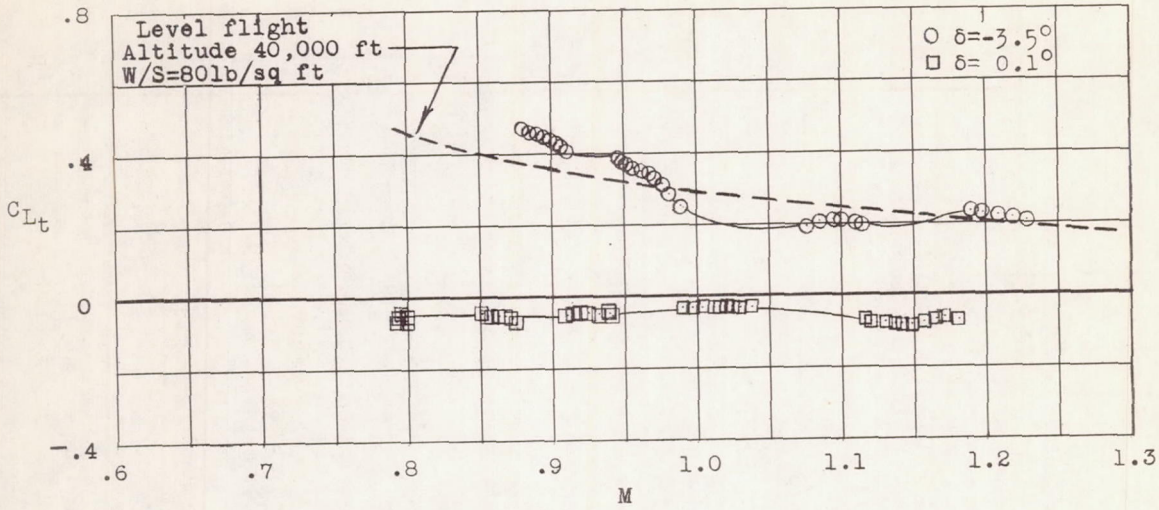

(a) Trim lift coefficient plotted against Mach number.

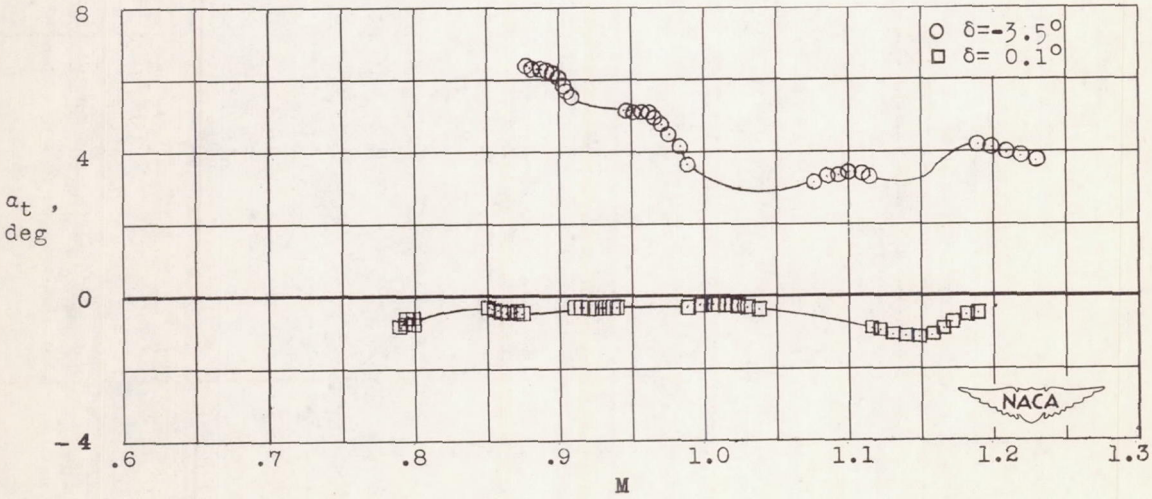

(b) Trim angle of attack plotted against Mach number.

Figure 23.- Trim characteristics.

NACA-Langley - 1-4-54 - 325

CONFIDENTIAL

CONFIDENTIAL